Cellulose (2022) 29:2145–2158
https://doi.org/10.1007/s10570-022-04449-1

ORIGINAL RESEARCH

Mechanism of moisture adsorption in plant fibers surface-modified with glycerol evaluated by LF-NMR relaxation technique

Lili Fu · Ke Zhang · Mingjian Zhang · Le Wang · Songjin Zheng · Ze Liu · Shanzhai Shang · Yue Sun · Feng Huang · Shuang Wang · Qi Zhang · Bing Wang · Bin Li · Yan Cao · Zhongya Guo

Received: 30 August 2021 / Accepted: 19 January 2022 / Published online: 4 February 2022

Abstract Surface modification by humectants is an important technology to improve product quality in textile field, healthcare, tobacco processing and paper-making industry. As a common humectant glycerol is applied to keep the moisture adsorbability of the plant fibers during manufacturing. The effects of glycerol on the moisture adsorption of the plant fibers were studied by analyzing the induced differences of bulk and surface physicochemical property with XRD, FTIR, SEM characterizations. The improvement of moisture adsorption capacity of the modified plant fibers was caused by the increased active adsorption sites, while the moisture diffusion resistance increased simultaneously with glycerol indicated by a declining D_{eff}. LF-NMR relaxation spectra demonstrated the water state and distribution in the plant fibers were changed by loading glycerol. The moisture transfer mechanisms induced by glycerol were also investigated. Free water failed to materialize in the plant fibers treated with glycerol, immobile water existed preferentially during the adsorption, and bound water presented increasing after the immobile water was saturated. These findings are referenced values to improve the manufacturing processes of moisture-retaining properties of different functional plant fibers.

Supplementary Information The online version contains supplementary material available at https://doi.org/10.1007/s10570-022-04449-1.

L. Fu · K. Zhang · M. Zhang · L. Wang · Y. Sun · F. Huang · S. Wang · Q. Zhang · B. Wang · B. Li · Z. Guo (✉)
Zhengzhou Tobacco Research Institute of CNTC, Zhengzhou 450001, China
e-mail: zhongyaguo@126.com

L. Fu · Y. Cao
Guangzhou Institute of Energy Conversion, Chinese Academy of Sciences, Guangzhou 510640, China

S. Zheng
China Tobacco Hebei Industrial Co. Ltd, Shijiazhuang 050051, China

Z. Liu · S. Shang
China Tobacco Yunnan Industrial Co. Ltd, Kunming 650202, China

Graphical abstract

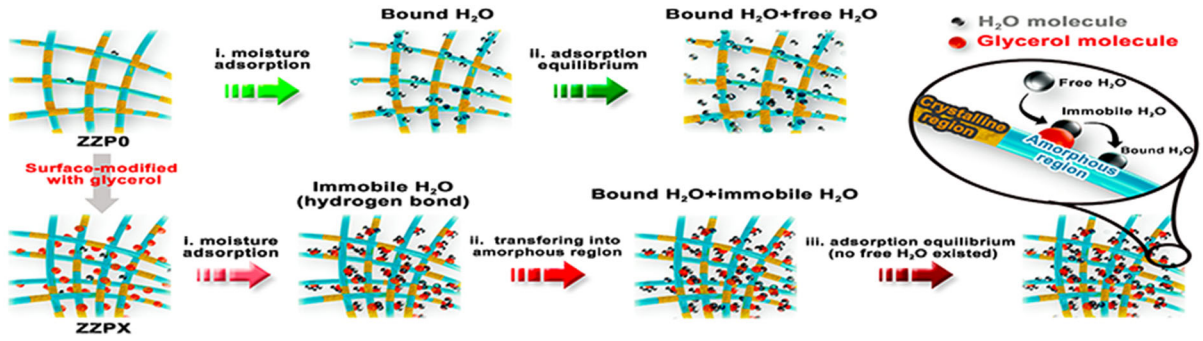

Keywords Moisture transfer · Plant fiber · LF-NMR relaxation technique · Water state and distribution

Introduction

Plant fibers contain major components of cellulose (linear polymers of glucose residues), hemicellulose (heteroglycans) and lignin (Pei and Ping 2012). Because of the rich hydrophilic functional groups of the former two components (Jiang et al. 2017; Hofstetter et al. 2006), the plant fibers present strong hydrophilic properties. Water adsorption capability of the plant fibers is closely related to their properties, such as mechanical strength (Perrier et al. 2017; Ridzuan et al. 2016), physicochemical resistance (Varara et al., 2018), bacterial inhibition capability (Popescu et al. 2014), hydrolysis (Jiang et al. 2021) and pyrolysis performance (Sun et al. 2019). Therefore, the water adsorption behaviour on plant fibers is importantly correlated to their wide applications, such as fields of paper-making (Modaressi and Garnier 2002), bio-energy (Emerson et al. 2018; Sotannde et al. 2020), bio-degradation (Gheorghita et al. 2020), functional materials (Hachem et al. 2020; Melo et al. 2021), pharmaceutics, cosmetics, textile and tobacco industries (Sun et al. 2019).

The moisture adsorption performances of plant fibers are mainly affected by hydrophilic compositions, microstructures and surface morphologies (Penttilä et al. 2020; Jiang et al. 2021), which can be changed by a multiple physiochemical methods and techniques.

Researchers have investigated on the surface modification with humectants to optimize the moisture adsorption property and strengthen the water holding capacity (WHC) of the plant fibers (Jiang et al, 2021; Yamamoto et al. 2020; Wang et al. 2020b). Among of them, glycerol is commonly applied as a humectant in textile field, healthcare, tobacco processing and paper-making industry. For example, a sheet of the plant fibers coated with a high spreading rate (20–30%, 80% of the coating liquid being glycerol) is used for producing ultra-soft moisture tissue towel paper with outstanding features of hydrophilicity, excellent softness and skin-friendliness for newborns and other special populations. In tobacco industry, glycerol is usually used as a humectant added into the heated tobacco substrate to preserve its moisture content and generate aerosol when it was heated (Yang et al. 2015; Halter and Ito 1972). Overall, investigations of mechanisms on WHC of the plant fibers loaded with glycerol were limited, given their importance and the demands for the optimization.

The moisture adsorption of plant fibers is affected by the interaction between their equilibrium adsorption capacity and transport resistance (Alak et al. 2000). Water vapor adsorption experiments could reveal the influence of glycerol on hygroscopic kinetic parameters. Low-field nuclear magnetic resonance (LF-NMR) technique has been widely used in obtaining the water state and distribution in different materials, such as fruits, vegetables, protein, woods and other porous media. Relaxation time demonstrates variations of physical and chemical processes of the inter-facial water from the perspective of molecular structure. Two-dimensional time domain LF-NMR

(2D LF-NMR) technique (Guo et al. 2019; Wang et al. 2020b; Montrazi et al. 2018; Zheng et al. 2017) combining two sequences between longitudinal (lattice-spin relaxation time, T_1) and transverse (the spin–spin relaxation time, T_2) relaxation time (T_1–T_2) simultaneously has been developed. Among the parameters, T_1 is the time for the protons to relapse to the original energy stage while the additional pulse electromagnetic wave is removed, and T_2 is the time for the actuated protons in the identical frequency but different moving tends to change their directions at the same level (Joardder et al. 2019; Wang et al. 2020a). 2D LF-NMR offers an enhancement to basic 1D technique, and the result could be presented as 2D correlation maps of T_1–T_2 relaxation spectra after 2D inverse Laplace transforms of the original data. According to the BPP theoretical model (Merobbie et al. 2007), T_1 is closely related to the motion of molecules and easily affected by the exchange process between the different protons, and suitable for the study of the high-frequency motion in the system, and T_2 is affected by the dipolar coupling between protons. The sequence for capturing T_1 data is encoded in the indirect dimension, while that for T_2 is modulated by the direct dimension. Inversion-Recovery (IR) and Saturation-Recovery (SR) are encoded in the indirect dimension for T_1, and encoded in the combination with Carr-Purcell-Meiboom-Gill (CPMG) for T_2. Thus, protons can be distinguished to several components by the value of the relaxation time in samples, leading to the capture and visualization of existing states and distributions of water in samples during the water vapor adsorption (Sanders et al. 2021).

Although the moisture adsorption of the porous media has been studied for more than a century, researchers have not reached a consensus on the mechanism of the water migration (Popescu et al. 2014; Hill et al. 2009) and proposed numerous adsorption mechanisms (Fredriksson and Thybring 2018; Guo et al. 2017; Lovikka and RautkariL 2018; Zhang et al. 2018), such as the moisture transfer process via the mono-layer adsorption, the muti-layer adsorption or the capillary condensation upon the increased relative humidity, parallel exponential kinetics. This work applied the advanced and insightful 2D LF-NMR technique to study the water state and distribution of the plant fibers loaded with glycerol. Some characterization methods were applied to demonstrate the change of the pore structure and surface of these samples. In the water vapor adsorption experiment, the influence of glycerol on hygroscopic kinetic parameters was revealed. The collected information was aimed to provide the establishment of mechanisms on the moisture migration in the plant fibers.

Materials and methods

Sample preparation

In this study, a plant fiber sheet (coded as ZZP0) is produced by China Tobacco Yunnan Reconstituted Tobacco Co. Ltd. ZZP0, plant-sourced material consisted of wood pulp and hemp pulp at 90–98% to 2–10%, and the ratios of cellulose, hemicellulose and lignin are 52.8%, 30.5% and 16.8% respectively. ZZP0 exhibits paper structure with a finished surface density of 45 ± 0.5 g/m^2.

This sample was subjected to post-treatments using a set of self-designed devices to impregnate glycerol first and followed by a two-stage infrared drying process (Fig. 1). The impregnation liquid was made of glycerol-ethanol solution, and the two-stage infrared was conducted at 50 °C and 80 °C in order.

The composite sheet samples loaded with different glycerol contents were coded as ZZP1, ZZP2 and ZZP3. They were obtained by adjusting the concentration of the applied impregnation liquid. Glycerol content of the sample was analyzed by gas chromatography (GC 6890, Agilent Technologies, Inc. US). The information of the starting material ZZP0 and its post-treatment samples ZZP1, ZZP2 and ZZP3 is given in Table 1.

Besides all of the samples were used during the water vapor adsorption, characterization and LF-NMR T_2 relaxation spectra, ZZP0 and ZZP3 were applied for capturing 2D LF-NMR T_1-T_2 relaxation spectra. Each sample sheet was cut into 0.5 × 0.5 cm in size for the subsequent characterizations and experiments except for the air permeability measurement.

Water vapor adsorption experiment

The moisture adsorption properties of the series samples were measured using a water vapor sorption kit called SPSx-1μ Advance (ProUmid GmbH & Co. KG, Germany). Samples were placed on the sample

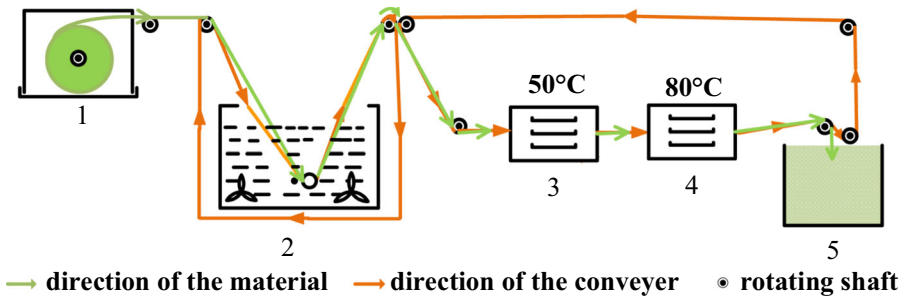

Fig. 1 The experimental set-up used for drying and impregnating device: 1—raw material tank (plant fiber sheet roll); 2—impregnating device; 3,4—infraed drying; 5—post-treated sample collector

Table 1 Information of the plant fiber samples

Sample	Preparation condition		wt%	L′ (mm)
	c_{is} (mol/L)	t_i (min)		
ZZP0	–	–	0.00	0.120
ZZP1	0.20	1	5.60	0.131
ZZP2	0.60	5	14.12	0.135
ZZP3	1.00	5	21.02	0.137

c_{is} is the molar concentration of glycerol in impregnating solution, mol/L; t_i is the immersion time of plant fiber, min; *wt*% is the mass percent of glycerol in the plant fibe; $L^{'}$ is the thickness of the sample, mm

holder that was connected to a microbalance under a hanging wire. The holder was located in a thermostatically controlled chamber, which provides a stable hygrothermal environment (Alak et al. 2000; Guo et al. 2017). Prior to the water vapor adsorption of plant fiber samples at a specific condition of 25 °C and 80% RH (relative humidity), samples were conditioned at 25 °C and 0% RH for 24 h. The judgement of the adsorption equilibrium was that the rate of the sample mass change was below 0.2 mg/20 min.

In this work, the moisture content (*MC*) was the water content on dry weight base, and the calculation of moisture ratio (*MR*) of each sample followed the Eq. (1) (Chen et al. 2012):

$$MR = \frac{MC_e - MC_t}{MC_e - MC_0} \quad (1)$$

where MC_t is the real-time (t, s) moisture content (%), MC_0 is the initial moisture content (%), and MC_e is the equilibrium adsorption moisture content (%).

The equation Eq. (2) below, based on Fick's Second Law of diffusion was applied for the calculation of the effective diffusivity of the samples (Chen et al. 2012). D_{eff} was determined by the slope of the straight line of experimental adsorption data in terms of ln(*MR*) vs. adsorption time, whereas the *MR* value $\geq$ 0.05 was applicable to fit the line.

$$\ln(MR) = \ln\left(\frac{8}{\pi^2}\right) - \left(\frac{\pi^2 D_{eff}}{4L^2}\right) \quad (2)$$

where t is adsorption time (s), L is the half thickness of the sample (m), D_{eff} is the diffusion coefficient (m^2/s).

To capture the adsorption isotherms of the samples before and after loading with glycerol, the dynamic vapor sorption (single cycle adsorption–desorption) was carried out by SPSx-1μ Advance (Hill et al. 2010; Fredriksson and Thybring 2018; Guo et al. 2017) at 25 °C. The wide RH range was from 0 to 95%, and the judgement of the adsorption equilibrium for the target RH was consistent as mentioned above.

Sample characterizations

Crystal structures of the plant fibers with the loaded glycerol were explored using a X-ray diffractometry (D8 Advance, Bruker Corporation, Germany), the laboratory X-ray generator operating in reflection mode. The maximum power, tube voltage and electric current of the X-ray emitter were 3 KW, 40 kV and 40 mA, respectively. The sample holder is made of single crystal silicon (20 mm diameter, 0.5 mm thickness), the scanning angle 2θ ranged from 5° to 50°, and all 2θ values are from Cu Kα radiation. ZZP0 is made from wood and hemp pulp, exhibiting paper structure, to avoid the the effect of ball milling on the crystallinity index (CrI) of the samples, all sample sheets were cut into pieces 0.5 × 0.5 mm in size for this characterization. Surface functional groups of samples were determined using a FTIR spectroscopy (IS 50, Thermo Scientific Nicolet, USA). The spectra were recorded in the range of 400–4000 cm^{-1} and

each spectrum was the result of 32 accumulated scans with 4 cm^{-1} resolution. The pore characteristics of the samples were investigated by a *mercury intrusion porosimetry* (MIP) (AutoPore IV 9500, Micromeritics Instrument Corporation, US). The observation was carried after the samples underwent drying process at 80 °C, 2 h. Air permeability was analyzed by an air permeability tester (TQY-4A, Hefei Institutes of Physical Science, China Academy of Sciences, China). Morphology and composition spectral analysis on the samples were observed by a field emission scanning electron microscopy (SEM, ZEISS Sigma 300, Carl Zeiss AG, Germany) operating at 20.0 kV. Each sample was mounted on a sample holder with the carbon conductive tape and coated with a thin layer of platinum using a sputter coater.

The water state and distribution in the samples were performed using a LF-NMR analyzer (NMI20-040 V-I, Shanghai Niumag Co., Ltd, China), equipped with a 0.55 T permanent magnet corresponding to a proton resonance frequency of 22.4 MHz at 30 °C. 2D LF-NMR T_1-T_2 relaxation spectra on ZZP0 and ZZP3 were collected based on the SR-CPMG sequence in a Teflon sample tube (φ40 mm, internal diameter). To increase the ratio of signal-to-noise (S/N), the relaxation data were measured from 2000 echoes with 9 μs and 25 μs for 90° and 180° pulses respectively. Other test parameters included: 0.1 ms for echo time, 10 dB and 3 dB for analog gain and the digital gain respectively, 32 for the number of repeat scanning (NS), 1000 ms for waiting time (TW), 200 kHz for sampling frequency (SW). T_2 relaxation spectra were collected based on the CPMG pulse sequence. The parameter setting was consistent to the 2D LF-NMR T_1-T_2 relaxation spectra test above. Multi-ExpInv analysis software (Shanghai Niumag Co., Ltd, China) was applied during the signal value inversion.

Results and discussion

Water vapor adsorption dynamics of the plant fibers

Water vapor adsorption experiments were conducted at 25 °C and 80% RH, and the moisture adsorption curves of the experimental samples were shown in Fig. 2a. It exhibited the corresponding increase of MC_e with the increasing content of glycerol, evidenced by 14.22%, 19.64%, 25.03% and 34.41% for ZZP0, ZZP1, ZZP2 and ZZP3, respectively. The prolonged hygroscopic equilibrium time was another marker by the increased application content of glycerol, evidenced by that 8.38 h for ZZP0 and 18.37 h for ZZP3 (2.19 times). According to Eq. (2), the adjusted R-square of the fitting line correlating ln*(MR)* and the time was greater than 0.994 for each sample (Fig. 2b). The calculated D_{eff} values were 1.841×10^{-13} m^2/s, 1.565×10^{-13} m^2/s, 1.391×10^{-13} m^2/s and 1.255×10^{-13} m^2/s for ZZP0, ZZP1, ZZP2 and ZZP3, respectively, revealing a decrease of D_{eff} upon the increased content of glycerol. The moisture capacity strengthened while the D_{eff} of moisture decreased during the moisture adsorption in the plant fibers. Fig. S1 displayed the MC_e of the samples enhanced with the increase of the glycerol content especially at RH higher than 60% RH. According to the International Union of Pure and Applied Chemistry (IUPAC) classification, as shown in Fig. S1a, the moisture adsorption of ZZP0 was characterized by the sigmoidal shape (type II) isotherm (Hill et al. 2010; Popescu et al. 2014) and an absolute hysteresis was observed around 80% RH (Hill et al. 2010). In contrast, the adsorption isotherms of ZZP2-3 (Fig. S1c-d) conformed to type III (Popescu et al. 2014), and the hysteresis phenomenon barely existed for ZZP2-3. Hill et al. (2010) verified that glycerol applied as a humectant changed the moisture adsorption property of the plant fibers and the interaction mechanisms between water vapor and the samples, concluding that reversible formation of hydrogen bonding occurred during the moisture adsorption for the plant fibers with glycerol.

The distributed water adsorption sites existing in the amorphous region (Garg et al. 2021) and the amount of hydrophilic functional groups significantly influenced the moisture adsorption performance of the plant fibers. The moisture diffusion resistance during the adsorption process was associated with the pore characteristics and permeability of the plant fibers (Jiang et al. 2017).

As a major *component* of the plant fibers, cellulose contains a crystalline structure with intra- and intermolecular hydrogen bonds (Dereka et al. 2021). Water molecules on the plant fibers are linked to their amorphous region by the hydrogen bond. Figure 3 shows XRD patterns of all the samples. The background signal including the sample holder and basal

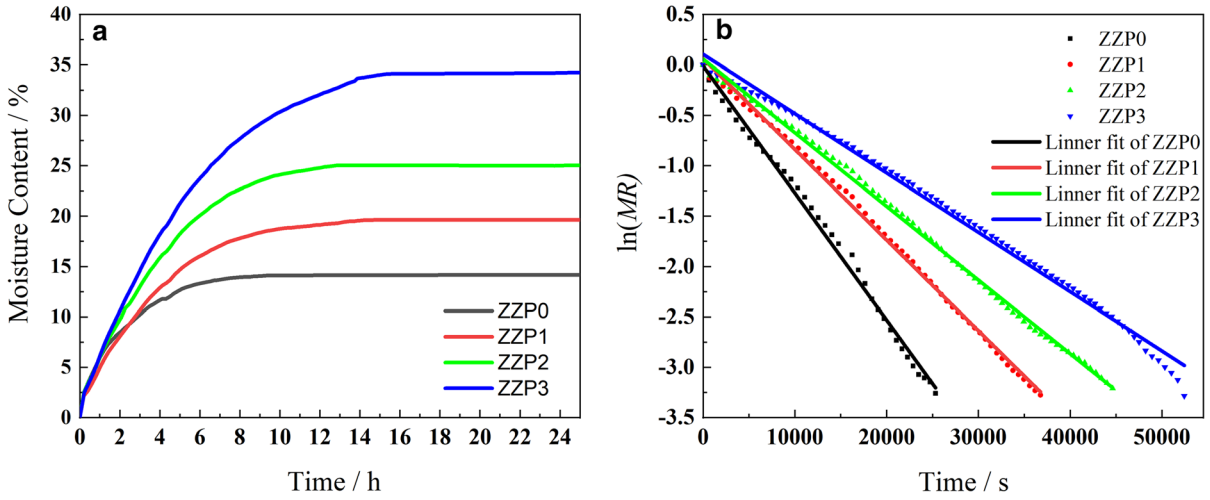

Fig. 2 Moisture adsorption curves of the samples (**a**) and correlation between ln(*MR*) vs. the adsorption time (**b**)

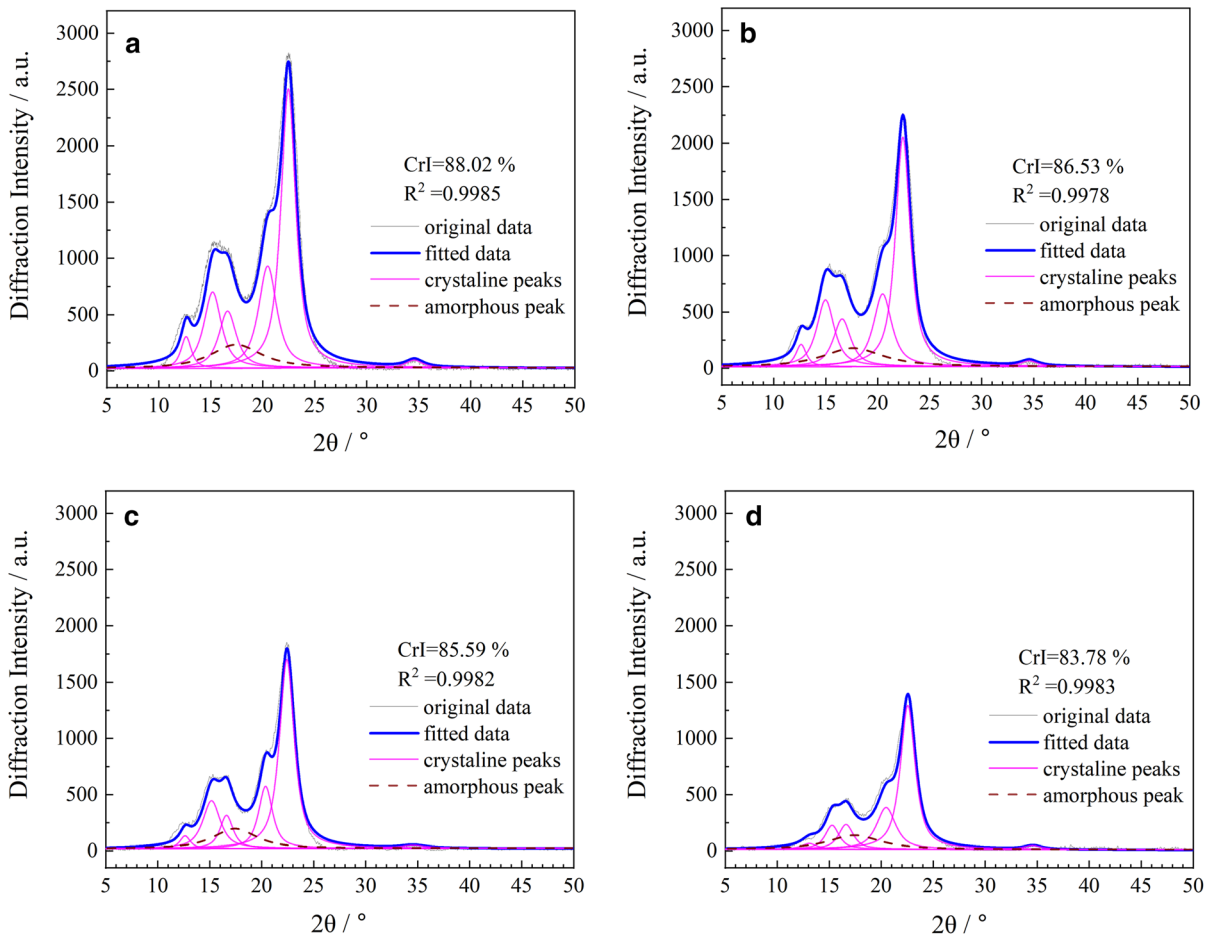

Fig. 3 Peak deconvolution of the plant fiber samples XRD data: (**a**) ZZP0; (**b**) ZZP1; (**c**) ZZP2; (**d**) ZZP3

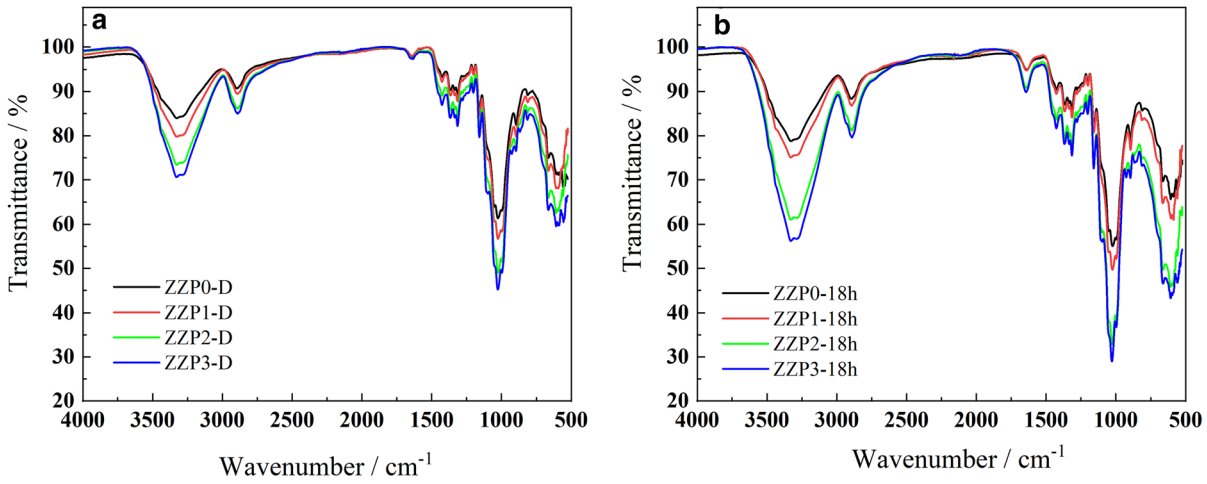

Fig. 4 IR spectra of the dried (**a**) and hygroscopic (**b**) plant fiber samples

signal should be subtracted from XRD data to optimize the fitting progress, and this measure could ensure a stable baseline fitting, demonstrating the XRD patterns with nearly zero intensity at 30° 2θ (Fig. 3). The XRD patterns presented peaks at 15.04°, 16.04° and 22.49° 2θ, which were assigned to that the Miller indices of (1–10), (110) and (200), respectively, typical of cellulose Iβ (French 2014; Wang et al. 2016). Additionally, the indices of (1–10) and (110) for the peaks at 12.16° and 20.34° 2θ, respectively, indicated the presence of cellulose II (French 2014). Hence, ZZP0-3 presents the crystalline structure of cellulose I and II. Because of the presence of cellulose II, Segal equation is not appropriate to calculate the CrI of the samples (French and Santiago Cintrón 2013; French 2020), deconvolution method with Voigt function (Yao et al. 2020) representing the separate peaks associated with crystalline structures and amorphous region was proposed to analyze the CrI of the samples. Figure 3 showed that CrI decreased from 88.02% to 83.78% upon the increase of glycerol content and the R^2 of the fitting for every sample was above 0.9978. This was likely caused by glycerol enlarging the amorphous region but not the crystalline regions or the surface morphology (see Fig. S2). The enlarged amorphous region promoted the WHC of the plant fibers.

The hydroxyl group in glycerol seemed to have contributed to the formation of hydrogen bond between the water molecule and the sample. Both the hydroxyl group and the *MC* were positively correlated with the glycerol content during the water vapor adsorption. For example, ZZP3 had the highest glycerol content and the MC_e value. FTIR spectroscopy could reveal the presence of organic functional groups in the plant fibers (see Fig. S3 and Table S1), especially the existence of hydrogen bonding structures which agreed with the literature on this type of materials (Bu et al. 2018). As shown in Fig. 4, the wide band at 3330 cm^{-1} could be attributed to –OH vibrational stretching (Bu et al. 2018; Kolbuk et al. 2020), 2900 cm^{-1} to –CH stretching, 997 cm^{-1} to methylene ($–CH_2–$), 1051 cm^{-1} to methine and 1025 cm^{-1} to the alcoholic hydroxyl vibration (C–OH) (Lorenzo et al. 1999), respectively. The peaks at 2900 cm^{-1}, 997 cm^{-1}, 1051 cm^{-1} and 1025 cm^{-1} were enhanced, and the absorption ranges of 3260–3330 cm^{-1} representing the inter-molecular hydrogen bonds (H-bonds) (Liu et al. 2013; Xin et al. 2015) between the plant fiber and glycerol. The increasing water adsorption sites (Taniguchi et al. 1978) here were attributed to the existence of glycerol because of its dramatic hygroscopicity (Fig. 4a). ZZP3 presented dramatic increase of peak patterns at 3330 cm^{-1} and 1647 cm^{-1} after water vapor adsorption (Fig. 4b), the former was attributed to the inter-molecular hydrogen bonds (Liu et al. 2013; Xin et al. 2015) both in the water-glycerol system and the water-amorphous region of the plant fiber after ZZP1-3 experienced the water vapor adsorption, the later attributed to the H–O–H stretching of absorbed water (Dereka et al. 2021), and the WHC of the plant fibers was promoted due to the existence of glycerol, which caused the increase of the interaction in the water-

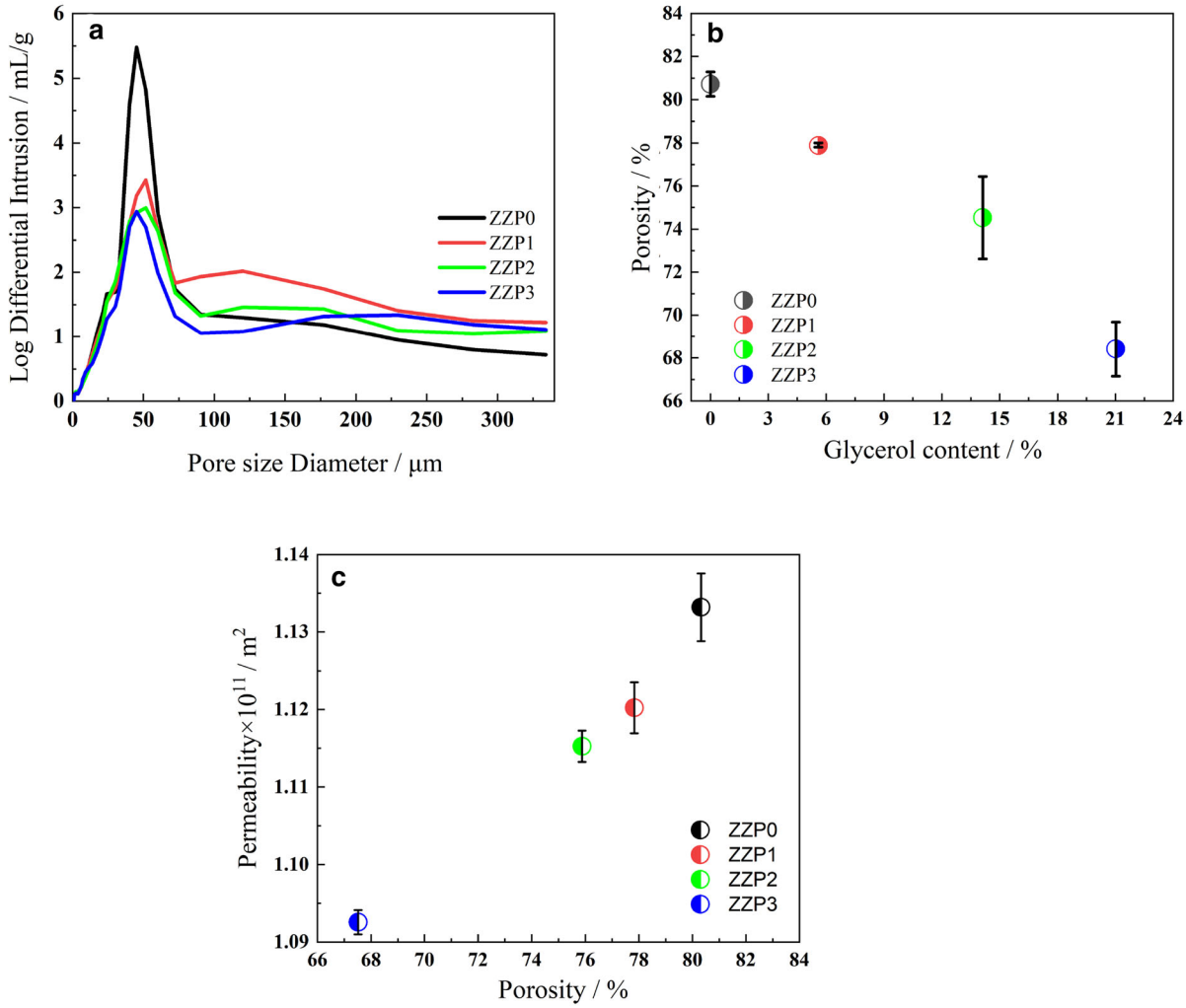

Fig. 5 The aperture distribution of the samples (**a**); the relationship between the porosity and glycerol content (**b**); the relationship between the permeability and the porosity (**c**)

glycerol-plant fiber system, including hydrogen bonds and adsorption sites, particularly the hydrogen bonds between glycerol and water.

These findings showed that loading with glycerol extended the equilibrium time and decreased D_{eff} of the plant fibers (Fig. 2). It could be deduced that outstanding moisture capacity cost longer equilibrium time during the water vapor adsorption, and the added glycerol enhanced the water transport resistance due to the change of pore characteristics (possibly pore structure, pore size or porosity) and the water permeability of the plant fibers.

According to Fig. 5a, the samples demonstrated macroporous structure (25–75 μm, dominantly) by MIP, and loading of glycerol reduced the porosity of the plant fibers. ZZP1 indicated an obvious decline of macroporous proportion comparing with ZZP0, while the macroporous proportion of ZZP2 and ZZP3 reduced gradually comparing with ZZP1 (Fig. 5a). The porosity values were 80.32%, 77.83%, 75.88% and 67.52% for ZZP0, ZZP1, ZZP2 and ZZP3, respectively (Fig. 5b). By inference, some glycerol molecules impregnated into the macropore preferentially during the impregnation, and the others possibly binded to the surface of the plant fibers. Glycerol occupied part of the pore volume, and the fiber layers wrapped with glycerol extended the path of water molecules in further during the water vapor

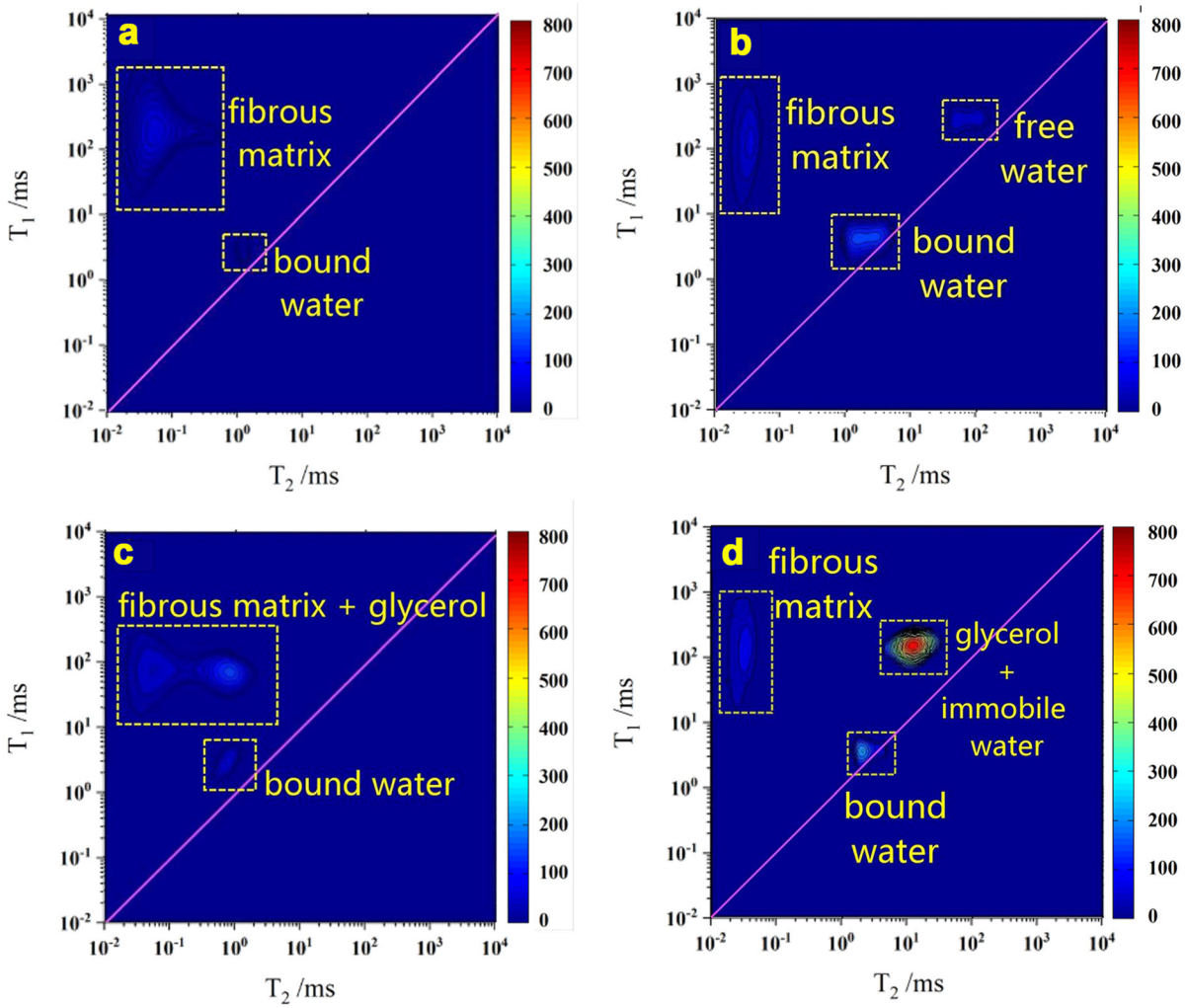

Fig. 6 2D LF-NMR T_1–T_2 correlation relaxation spectra of ZZP0 (**a**) and ZZP3 (**c**) after drying treatment at 80 °C, 0% RH, for 2 h; ZZP0 (**b**) and ZZP3 (**d**) after hygroscopic treatment at 25 °C, 80% RH, for 18 h. T_2 relaxation time is given in X axis and T_1 relaxation time in Y axis

adsorption. The permeability of the sample reflected the mass transport capacity of the sample (Liu et al. 2006), and the values were 1.13628×10^{-11} m^2, 1.1179×10^{-11} m^2, 1.11382×10^{-11} m^2 and 1.09365×10^{-11} m^2 for ZZP0, ZZP1, ZZP2 and ZZP3, respectively. The porosity of the plant fibers decreased with the increase of glycerol content (Fig. 5b), and the decline of macroporous proportion and porosity (Fig. 5c) caused the permeability reduction. These factors led to the rise in the water diffusion resistance of the plant fibers during the water vapor adsorption.

Effect of glycerol on the water state of the plant fibers

2D LF-NMR relaxation spectra reflect the change of water state and distribution (Melo et al., 2021) in the plant fibers caused by glycerol during the water vapor adsorption, SR-CPMG sequence was applied to capture 2D T_1-T_2 maps of the samples. Three main water states in the plant fibers could be distinguished clearly, according to the relaxation time of T_2. Specifically, the $T_{2\text{-b}}$ in the range of 0.02–10 ms (2×10^{-2}–1×10^{1} ms) and 0.02–5 ms (2×10^{-2}–5×10^{0} ms) were assigned as bound water (adsorbed *water*) for ZZP0 and ZZPX (the samples with glycerol)

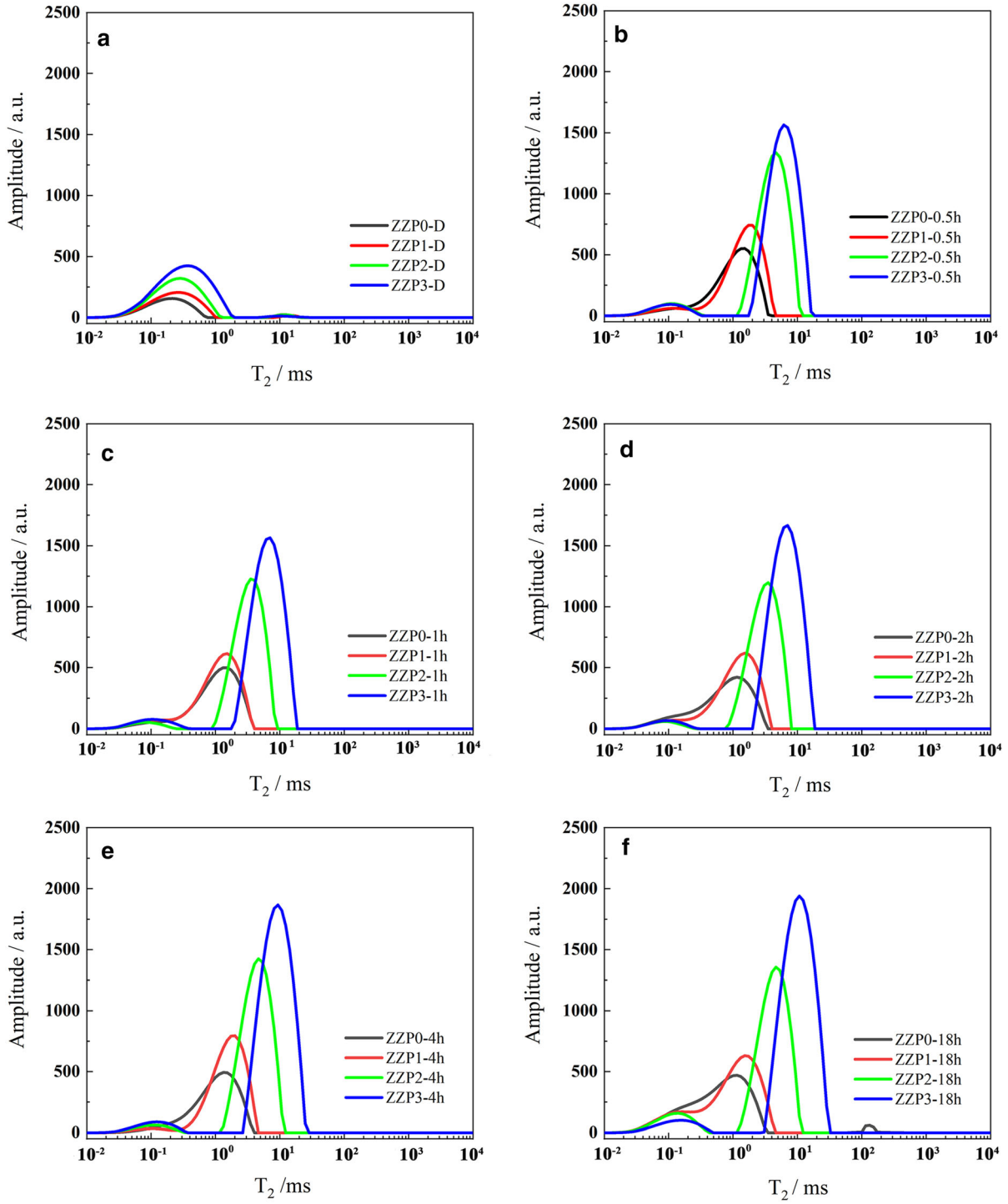

Fig. 7 T_2 relaxation spectra of the plant fiber samples after different treatments **a** drying treatment at 80 °C, 0% RH, for 2 h; **b–f** water vapor adsorption at 25 °C, 80% RH, for different time

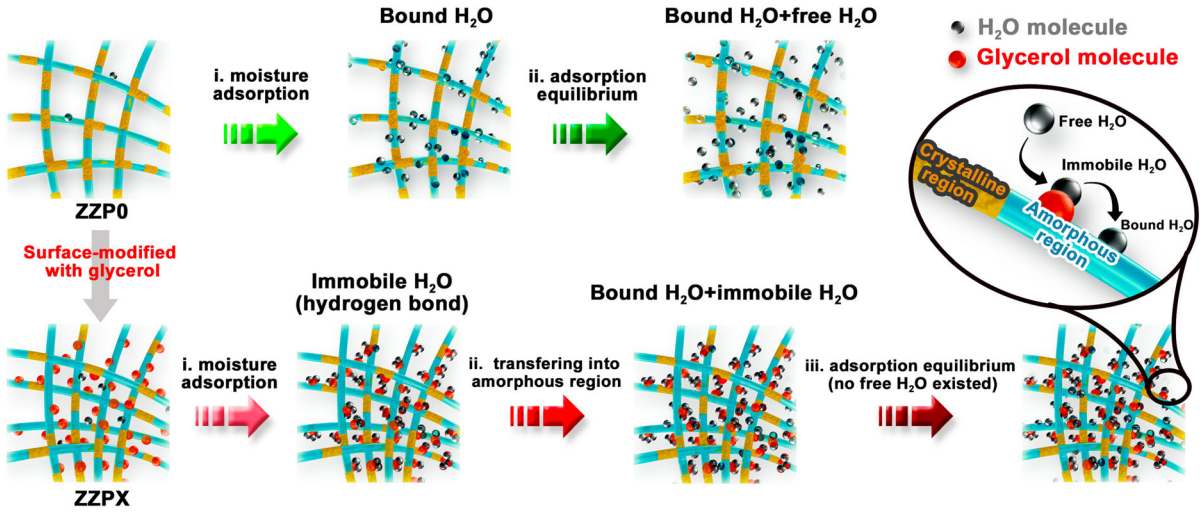

Fig. 8 The moisture adsorption process of the plant fibers before and after loading with glycerol

respectively, $T_{2\text{-i}}$ 5–80 ms (5×10^0–8×10^1 ms) as immobile water for ZZPX, and $T_{2\text{-f}} > 100$ ms (1×10^2 ms) as free water for ZZP0 ~ 3 in this manuscript. The immobile water ($T_{2\text{-i}}$) was a kind of intermediate water (Wang et al. 2020b) mixed with glycerol, representing the state between bound water and free water due to the hydrogen bonding caused by glycerol and water molecules.

ZZP0 in dry state presented a small amount of bound water (Yang et al. 2020) as shown in Fig. 6a, which $T_{2\text{-b}}$ was 0.21–2.5 ms (2.1×10^{-2}–2.5×10^0 ms). As water vapor adsorption time extended, bound water and free water coexisted in ZZP0, the former was given priority. Figure 6b presented that there were bound water $T_{2\text{-b}}$ 0.21–2.5 ms (2.1×10^{-2}–2.5×10^0 ms) mainly, free water $T_{2\text{-f}}$ 80–193 ms (8×10^1–1.92×10^2 ms) partially when ZZP0 achieved to moisture adsorption equilibrium. This result was similar to other biomass and porous media for water vapor adsorption (Wang et al. 2020b).

ZZP3 showed differences in water state and its distribution compared with ZZP0 at dry state. The proton signal of glycerol and fibrous matrix overlapped partly due to the interaction between them, and merely bound water $T_{2\text{-b}}$ 0.021–3.5 ms (2.1×10^{-2}–3.5×10^0 ms) existed in ZZP3 at the dry state (Fig. 6c). The outstanding hydrophilicity of glycerol was proved according to Fig. 6d, indicating that the proton signals of glycerol and immobile water were indivisible when ZZP3 attained moisture adsorption equilibrium. Even the WHC of the samples improved significantly, there was no free water existing in the plant fibers loaded with glycerol.

Figure 7a indicated that there was a small amount of water left in per sample and the *MC* was proportional to the content of glycerol at the dry state. ZZP0 demonstrated the lowest intensity, and $T_{2\text{-b}}$ 0.21–2.5 ms (2.1×10^{-1}–2.5×10^0 ms) represented bound water only, while the other samples contained bound water and immobile water mixed with glycerol whose intensity was detected at $T_{2\text{-i}}$ 10–35 ms (1×10^1–3.5×10^1 ms). The amount of bound water heightened with the increase of glycerol content, while their immobile water decreased after the samples dried for 2 h at 80 °C and 0% RH. With the time of moisture adsorption extended at 25 °C and 80% RH, T_2 relaxation spectra of the four samples were shown in Fig. 7b-f respectively. The peak area of $T_{2\text{-i}}$ (immobile water mixed with glycerol) accounted for a major proportion and the amount of immobile water increased significantly, while the corresponding peak area of $T_{2\text{-b}}$ (bound water) was much less and increased slowly. With the MC of the samples enhanced, the value of relaxation time $T_{2\text{-i}}$ shifted to the right, especially for the high glycerol content samples ZZP2 and ZZP3. When the immobile water closed to the saturation point, the peak area of $T_{2\text{-i}}$ moved towards stability, and that of $T_{2\text{-b}}$ gradually enlarged until the moisture adsorption equilibrium was achieved. The result indicated the adsorption of bound water responded behind immobile water for the

plant fibers added with glycerol. When ZZP0 reached its moisture adsorption equilibrium, the free water distribution pattern of $T_{2\text{-f}}$ could be monitored (Fig. 7f), while no free water signal appeared in ZZP1-3. We postulated that water molecules entered the plant fibers with glycerol as immobile water preferentially during the water vapor adsorption, and when the immobile water molecules were closed to the saturation, part of them became bound water, simultaneously external water molecules supplemented the vacancy of immobile water until the bound and immobile water were saturated. During the whole adsorption process, the bound and immobile water were the main forms of water molecules for the plant fibers loaded with glycerol.

Moisture adsorption mechanisms of the plant fiber before and after loading with glycerol

Figure 8 illustrates the moisture adsorption behavior during the transfer of water molecules in ZZP0 and ZZPX loaded with an amount of glycerol. Comparing with ZZP0, glycerol decreased the porosity and CrI of the plant fibers, enlarged the amorphous region and increased the active adsorption sites due to intra- and inter-molecular hydrogen bonds for ZZPX. As a consequence, glycerol enhanced the MC_e of the plant fibers. However, it strengthened the moisture transport resistance (Alak et al. 2000) and caused a decrease of D_{eff}.

For ZZP0, as the moisture adsorption time extended, the water molecules entered the surface and amorphous region (Stevanic and Salmén 2020) of the plant fibers and transformed into bound water, *simultaneously* part of the water existed in the macropore of ZZP0 as free water. For ZZPX, water molecules entered the plant fibers as the immobile water preferentially, due to the hydrogen bond interaction between glycerol and water molecules. When the immobile water tended to be saturated, part of the immobile water acted with the amorphous region of the plant fibers and transformed into bound water, simultaneously external water molecules supplemented the vacancy of immobile water until the bound and immobile water were both saturated due to the hydrogen bond interaction between glycerol and water molecules.

Conclusions

The moisture adsorption sites of a plant-based composite fiber material were enhanced by glycerol loading, while the water diffusion resistance increased *simultaneously*. LF-NMR technique provides a new method to capture the mechanism of water vapor adsorption in the plant fibers before and after loading with glycerol. The technique revealed that glycerol could affect the water states and the distributions in the plant fibers with glycerol during the moisture adsorption. During the moisture adsorption, water molecules entered the plant fibers loaded with glycerol as immobile water preferentially because of the hydrogen bonds between water and glycerol molecules. Part of the immobile water transformed into bound water when the immobile water tended to be saturated, simultaneously external water molecules supplemented the vacancy of immobile water. No free water appeared during the whole moisture adsorption process of the plant fibers loading with glycerol. The research outcome expands the knowledge on moisture adsorption behavior of the plant fibers and their modification by adding humectants.

Acknowledgments The authors are extremely grateful for Dr Jiashi Wang and the engineer Danli He and Qi Zhou for their technical supports. At the same time, the authors take this opportunity to thank Dr Chuan Liu for providing language help.

Author Contributions Conceptualization: LF and YC; Investigation, methodology: LF, ZG, KZ and YS; Experiment: SZ, ZL and SS; Writing-original draft preparation: LF; Writing-review and editing: MZ, FH, SW and QZ; Supervision: BW, BL and YC.

Funding This work was supported by the Postdoctoral Program of Zhengzhou Tobacco Research Institute of CNTC (China) and Fundamental Research Program of China Tobacco Yunnan Industrial Co. Ltd (2021XY01).

Declarations

Conflict of Interest The authors declare that they have no conflict of interest.

References

Alak B, Hari R, Bandru R, Siddharth C (2000) Moisture sorption response of paper subjected to ramp humidity changes: modeling and experiments. Ind Eng Chem Res 39:219–226. https://doi.org/10.1021/ie990279w

Bu X, Pei JC, Zhang FD, Liu HT, Zhou ZM, Zhen XQ et al (2018) The hydration mechanism and hydrogen bonding structure of 6-carboxylate chitooligosaccharides superabsorbent material prepared by laccase/TEMPO oxidation system. Carbohydr Polym 188:151–158. https://doi.org/10.1016/j.carbpol.2018.01.099

Chen DY, Zheng Y, Zhu XF (2012) Determination of effective moisture diffusivity and drying kinetics for poplar sawdust by thermogravimetric analysis under isothermal condition. Bioresour Technol 107:451–455. https://doi.org/10.1016/j.biortech.2011.12.032

Dereka B, Yu Q, Lewis NHC, Carpenter WB, Bowman JM, Tokmakoff A (2021) Crossover from hydrogen to chemical bonding. Science 371:160–164. https://doi.org/10.1126/science.abe1951 (PMID:33414217)

Emerson RM, Hernandez S, Williams CL, Hartley DS (2018) Improving bioenergy feedstock quality of high moisture short rotation woody crops using air classification. Biomass Bioenergy 117:56–62. https://doi.org/10.1016/j.biombioe.2018.07.015

Fredriksson M, Thybring EE (2018) Scanning or desorption isotherms? Characterising sorption hysteresis of wood. Cellulose 25:4477–4485. https://doi.org/10.1007/s10570-018-1898-9

French AD (2014) Idealized powder diffraction patterns for cellulose polymorphs. Cellulose 21:885–896. https://doi.org/10.1007/s10570-013-0030-4

French AD (2020) Increment in evolution of cellulose crystallinity analysis. Cellulose 27:5445–5448. https://doi.org/10.1007/s10570-020-03172-z

French AD, Santiago Cintrón M (2013) Cellulose polymorphy, crystallite size, and the Segal Crystallinity Index. Cellulose 20:583–588. https://doi.org/10.1007/s10570-012-9833-y

Garg M, Apostolopoulou-Kalkavoura V, Linares M et al (2021) Moisture uptake in nanocellulose: the effects of relative humidity, temperature and degree of crystallinity. Cellulose. https://doi.org/10.1007/s10570-021-04099-9

Gheorghita R, Gutt G, Amariei S (2020) The use of edible films based on sodium alginate in meat product packaging: an eco-friendly alternative to conventional plastic materials. Coatings 10:166. https://doi.org/10.3390/coatings10020166

Guo X, Wu Y, Xie X (2017) Water vapor sorption properties of cellulose nanocrystals and nanofibers using dynamic vapor sorption apparatus. Sci Rep 7:1–12. https://doi.org/10.1038/s41598-017-14664-7

Guo GF, Li B, Liu CX, Jin X, Wang ZG, Ding MZ et al (2019) Characterization of moisture mobility and diffusion in fresh tobacco leaves during drying by the TG-NMR analysis. J Therm Anal Calorim 135:2419–2427. https://doi.org/10.1007/s10973-018-7312-x

Hachem ZE, Célino A, Challita G, Branchu S, Duigou AL, Fréour S (2020) Dimensional variation and evolution of mechanical properties of wet aged composites reinforced with flax fibers. J Compos Mater 0:1–18. https://doi.org/10.1177/0021998320966045

Halter HM, Ito TI (1972) Reconstituted tobacco-smoking and health possibilities. J Natl Cancer Inst 48:1869–1883

Hill CAS, Norton A, Newman G (2009) The water vapor sorption behavior of natural fibers. J Appl Polym Sci 112:1524–1537. https://doi.org/10.1002/app.29725

Hill CAS, Norton A, Newman G (2010) The water vapour sorption properties of Sitka spruce determined using a dynamic vapour sorption apparatus. Wood Sci Technol 44:497–514. https://doi.org/10.1007/s00226-010-0305-y

Hofstetter K, Hinterstoisser B, Salmén L (2006) Moisture uptake in native cellulose-the roles of different hydrogen bonds: a dynamic FT-IR study using Deuterium exchange. Cellulose 13:131–145. https://doi.org/10.1007/s10570-006-9055-2

Jiang L, Wu N, Zheng A, Liu A, Zhao Z, Zhang F et al (2017) Comprehensive utilization of hemicellulose and cellulose to release fermentable sugars from corncobs via acid hydrolysis and fast pyrolysis. ACS Sustain Chem Eng 5:5208–5213. https://doi.org/10.1021/acssuschemeng.7b00561

Jiang XX, Zhai R, Jin MJ (2021) Increased mixing intensity is not necessary for more efficient cellulose hydrolysis at high solid loading. Bioresour Technol 329:1–10. https://doi.org/10.1016/j.biortech.2021.124911

Joardder M, Mourshed M, Masud MH (2019) Correction to: state of bound water: measurement and significance in food processing. (eBook). Spring, pp 47–76

Kolbuk D, Jeznach O, Wrzecionek M, Gadomska-Gajadhur A (2020) Poly (glycerol succinate) as an eco-friendly component of PLLA and PLCL fibres towards medical applications. Polymers 12:1–12. https://doi.org/10.3390/polym12081731

Liu W, Fan AW, Huang XM (2006) Theory and application of heat and mass transfer in porous media, 1st edn. Science Press, Beijing, pp 7–15

Liu DW, Yu Y, Wu HW (2013) Diffffferences in water-soluble intermediates from slow pyrolysis of amorphous and crystalline cellulose. Energy Fuels 27:1371–1380. https://doi.org/10.1021/ef301823g

Lorenzo MO, Haq S, Bertrams T, Murray P, Baddeley CJ (1999) Creating chiral surfaces for enantioselective heterogeneous catalysis: r, r-tartaric acid on Cu(110). J Phys Chem B 103:10661–10669. https://doi.org/10.1021/jp992188i

Lovikka VA, RautkariL MTC (2018) Changes in the hygroscopic behavior of cellulose due to variations in relative humidity. Cellulose 25:87–104. https://doi.org/10.1007/s10570-017-1570-9

Melo RQC, Fook MVL, Lima AGB (2021) Non-Fickian moisture absorption in vegetable fiber reinforced polymer

composites: the effect of the mass diffusivity. Polymers 13:1–30. https://doi.org/10.3390/polym13050761
Merobbie DW, Moore EA, Graves MJ et al (2007) MRI, from Ricture to Proton, 1st edn. Cambridge university Press
Modaressi H, Garnier G (2002) Mechanism of wetting and absorption of water droplets on sized paper: effects of chemical and physical heterogeneity. Langmuir 18:642–649. https://doi.org/10.1021/la0104931
Montrazi ET, Lucas-Oliveira E, Araujo-Ferreira AG, Barsi-Andreeta M, Bonagamba TJ (2018) Simultaneous acquisition for T_2–T_2 exchange and T_1–T_2 correlation NMR experiments. J Magn Reson 289:63–71. https://doi.org/10.1016/j.jmr.2018.02.008
Pei JC, Ping QW (2012) Lignocellulosic chemistry, 4th edn. China Light Industry Press, Beijing, pp 1–56
Penttilä PA, Altgen M, Carl N et al (2020) Moisture-related changes in the nanostructure of woods studied with X-ray and neutron scattering. Cellulose 27:71–87. https://doi.org/10.1007/s10570-019-02781-7
Perrier A, Touchard F, Chocinski-Arnault L, Mellier D (2017) Influence of water on damage and mechanical behaviour of single hemp yarn composites. Polym Test 57:17–25
Popescu CM, Hill CAS, Curling S, Ormondroyd G, Xie YX (2014) The water vapour sorption behaviour of acetylated birch wood: how acetylation affects the sorption isotherm and accessible hydroxyl content. J Mater Sci 49:2362–2371. https://doi.org/10.1007/s10853-013-7937-x
Ridzuan MJM, Abdul MMS, Afendi M, Azduwin K, Amin NAM, Zahri JM et al (2016) Moisture absorption and mechanical degradation of hybrid pennisetum purpureum glass-epoxy composites. Compos Struct 141:110–116. https://doi.org/10.1016/j.compstruct.2016.01.030
Sanders JM, Misra M, Mustard TJL, Giesen DJ, Zhang T, Shelley J et al (2021) Characterizing moisture uptake and plasticization effects of water on amorphous amylose starch models using molecular dynamics methods. Carbohydr Polym 252:1–11. https://doi.org/10.1016/j.carbpol.2020.117161
Sotannde OA, Dadile AM, Umar M, Idoghor SM, Zira BD (2020) Effect of fuel material compositions on combustion properties of wood chips from smallhold farm plots in a sudano-sahelian environment of nigeria. Curr J Appl Sci Technol 39:93–104. https://doi.org/10.9734/cjast/2020/v39i230502
Stevanic JS, Salmén L (2020) Molecular origin of mechano-sorptive creep in cellulosic fibres. Carbohydr Polym 230:1–6. https://doi.org/10.1016/j.carbpol.2019.115615
Sun Y, He Z, Tu R, Wu Y, Jiang E, Xu X (2019) The mechanism of wet/dry torrefaction pretreatment on the pyrolysis performance of tobacco stalk. Bioresour Technol 286:1–12. https://doi.org/10.1016/j.biortech.2019.121390
Taniguchi T, Harada H, Nakato K (1978) Determination of water adsorption sites in wood by a hydrogen-deuterium exchange. Nature 272:230–231. https://doi.org/10.1038/272230a0
Varara AK, Korneliya G, Nathalie L, Lennart B (2018) Thermal conductivity of hygroscopic foams based on cellulose nanofibrils and a nonionic polyoxamer. Cellulose 25:1117–1126. https://doi.org/10.1007/s10570-017-1633-y
Wang J, Li Y, Wang Z, Li Y, Liu N (2016) Influence of pre-treatment on properties of cotton fiber in aqueous NaOH/urea solution. Cellulose 23(3):2173–2183. https://doi.org/10.1007/s10570-016-0938-6
Wang H, Cui H, Wang X, Lin C, Zhang X (2020a) Metal complexed-enzymatic hydrolyzed chitosan improves moisture retention of fiber papers by migrating immobilized water to bound state. Carbohydr Polym 115967:1–10. https://doi.org/10.1016/j.carbpol.2020.115967
Wang SQ, Lin R, Cheng SS, Tan MQ (2020b) Water dynamics changes and protein denaturation in surf clam evaluated by two-dimensional LF-NMR T_1–T_2 relaxation technique during heating process. Food Chem 320:1–8. https://doi.org/10.1016/j.foodchem.2020.126622
Xin SZ, Yang HP, Chen YQ, Yang MF, Chen L, Wang XH, Chen HP (2015) Chemical structure evolution of char during the pyrolysis of cellulose. J Anal Appl Pyrolysis. https://doi.org/10.1016/j.jaap.2015.09.002
Yamamoto Y, Fujieda T, Ichiura H (2020) Reforming paper structure using an ionic liquid treatment to improve the specific surface area, moisture retention, and hydrophobicity. Cellulose 27:8317–8327. https://doi.org/10.1007/s10570-020-03303-6
Yang Q, Sun PZ, Fumagalli L, Stebunov YV, Haigh SJ, Zhou ZW et al (2020) Capillary condensation under atomic-scale confinement. Nature 588:250–253. https://doi.org/10.1038/s41586-020-2978-1
Yang J, Yang S, Duan YX, Tian YF, Zhao W (2015) Investigation of thermogravimetry and pyrolysis behavior of tobacco material in two heat-not-burn cigarette brands. Acta Tabacaria Sinica 21:7–13. https://doi.org/10.16472/j.chinatobacco.2015.070
Yao W, Weng Y, Catchmark JM (2020) Improved cellulose X-ray diffraction analysis using Fourier series modeling. Cellulose 27:5563–5579. https://doi.org/10.1007/s10570-020-03177-8
Zhang X, Li J, Yu Y, Wang H (2018) Investigating the water vapor sorption behavior of bamboo with two sorption models. J Mater Sci 53:8241–8249. https://doi.org/10.1007/s10853-018-2166-y
Zheng S, Li T, Li Y, Shi Q, Wu F (2017) Novel 1H NMR relaxometry methods to study the proton distribution and water migration properties of tobacco. Anal Methods 9:1741–1747. https://doi.org/10.1039/c6ay03242g